ORIGINAL ARTICLE

JBMR

Deficiency of Annexins A5 and A6 Induces Complex Changes in the Transcriptome of Growth Plate Cartilage but Does Not Inhibit the Induction of Mineralization

Daniele Belluoccio,[1] Ivan Grskovic,[2] Anja Niehoff,[3] Ursula Schlötzer-Schrehardt,[4] Sabrina Rosenbaum,[2] Julia Etich,[2] Christian Frie,[2] Friedericke Pausch,[5] Stephen E Moss,[6] Ernst Pöschl,[7] John F Bateman,[1] and Bent Brachvogel[2]

[1]Murdoch Childrens Research Institute and Department of Paediatrics, University of Melbourne, and Royal Children's Hospital, Parkville, Victoria, Australia
[2]Center for Biochemistry, Medical Faculty, University of Cologne, Germany
[3]Institute of Biomechanics and Orthopaedics, German Sport University, Cologne, Germany
[4]Department of Ophthalmology, University Erlangen-Nürnberg, Erlangen, Germany
[5]Department of Experimental Medicine I, Nikolaus-Fiebiger-Zentrum, University of Erlangen-Nürnberg, Germany
[6]Department of Cell Biology, Institute of Ophthalmology, University College London, London, United Kingdom
[7]School of Biological Sciences, University of East Anglia, Norwich, United Kingdom

ABSTRACT

Initiation of mineralization during endochondral ossification is a multistep process and has been assumed to correlate with specific interactions of annexins A5 and A6 and collagens. However, skeletal development appears to be normal in mice deficient for either A5 or A6, and the highly conserved structures led to the assumption that A5 and A6 may fulfill redundant functions. We have now generated mice deficient of both proteins. These mice were viable and fertile and showed no obvious abnormalities. Assessment of skeletal elements using histologic, ultrastructural, and peripheral quantitative computed tomographic methods revealed that mineralization and development of the skeleton were not significantly affected in mutant mice. Otherwise, global gene expression analysis showed subtle changes at the transcriptome level of genes involved in cell growth and intermediate metabolism. These results indicate that annexins A5 and A6 may not represent the essential annexins that promote mineralization in vivo. © 2010 American Society for Bone and Mineral Research.

KEY WORDS: ANNEXIN; MINERALIZATION; MICROARRAY; IN VIVO; EXPRESSION

Introduction

Members of the annexin protein family represent potential initiators of calcification within the growth plate during the formation of the mineralized skeleton.[1,2] Annexins are found in matrix vesicles that are released from terminally differentiated hypertrophic chondrocytes to the surrounding extracellular matrix, and these annexins may initiate calcium influx into the matrix vesicles. The increase of intravesicular calcium concentration in matrix vesicles induces the formation of hydroxyapatite crystals and cartilage mineralization. Owing to the affinity of annexin A5 (gene: *Anxa5;* protein: AnxA5) for phosphatidylserine-enriched matrix vesicles and for cartilage-specific collagens II and X, as well as its ability to form calcium-selective ion channels, it appeared to be the prototypical annexin for initiating calcium influx and mineralization.[3–5] AnxA5 greatly increases mineral formation when incorporated into synthetic nucleation complexes, and the interplay of AnxA5, collagen II, and collagen X enhances nucleation core formation in synthetic cartilage lymph and triggers apatite crystal formation during endochondral ossification.[6,7] Recently, Kirsch and coworkers speculated that the interactions between collagens and AnxA5 regulate the normal mineralization of growth plate cartilage as well as pathologic mineralization events.[8] This suggestion is consistent with the finding that AnxA5 is expressed not only in calcifying cartilage but also in perivascular cells of blood vessels, a cell type

Submitted for publication on 26 January 2009. Accepted in revised form on 24 March 2009. Published ahead of print on 6 July 2009.
Address correspondence to: Dr. Bent Brachvogel, Center for Biochemistry, Medical Faculty, University of Cologne, Joseph-Stelzmann-Str. 52, D-50931 Cologne, Germany. E-mail: bent.brachvogel@uni-koeln.de

Journal of Bone and Mineral Research, Vol. 25, No. 1, January 2010, pp 141–153
DOI: 10.1359/jbmr.090710

that is involved in ectopic calcification events in atherosclerosis.[9–11] The other two major annexins found in matrix vesicles, AnxA2 and AnxA6, also promote cartilage mineralization in vitro.[7,12] Despite these findings, there are no conclusive data to support the role of AnxA5 and AnxA6 during in vivo mineralization. In fact, analysis of mice single-deficient in AnxA5 or AnxA6 surprisingly displayed no obvious changes in skeletal development,[13–15] but growth plate development was not analyzed in detail. Structural and functional similarities between the annexins point to redundant functions of these proteins within the growth plate.[7,15]

To explore the role of AnxA5 and AnxA6 in biomineralization during endochondral bone formation and to address the possibility of functional redundancy, we developed and analyzed *Anxa5*$^{-/-}$*Anxa6*$^{-/-}$ double-deficient mice. We demonstrate that *Anxa5*$^{-/-}$*Anxa6*$^{-/-}$ mice were viable and fertile and displayed no alterations in development and maturation of the skeletal system. The potential interaction partners of the annexins in the extracellular matrix, collagen II and collagen X, as well as collagen-associated proteins such as cartilage oligomeric matrix protein (COMP) and collagen IX, are normally distributed within the juvenile growth plate. In contrast to collagen X–deficient mice,[16] no ultrastructural changes in matrix vesicle distribution were detectable in *Anxa5*$^{-/-}$*Anxa6*$^{-/-}$ mice. On the other hand, global transcriptome profiling of growth plate cartilage from mutant mice demonstrated specific changes in the expression of genes involved in cell growth and intermediate metabolism, whereas the expression of genes associated with the mineralization processes was unaltered. Whole-genome transcriptome profiling therefore points to a diverse function of both annexins in growth plate development.

Material and Methods

Mice

Anxa5$^{-/-}$*Anxa6*$^{-/-}$ mice were generated by intercrossing *Anxa5*[15] and *Anxa6* single-deficient mouse mutants.[13] Wild-type and mutant mice have a mixed genetic background of C57BL/6x129SvJ. Experiments were performed in accordance with the animal ethics guidelines of the Murdoch Children's Research Institute and the German animal protection law.

Genotype analysis

Genomic DNA were purified by standard methods and analyzed by polymerase chain reaction (PCR) using the following sets of primers for detecting the wild-type (*Anxa5Ex4dw:* 5′-GAAGCAATGCTCAGCGCCAGGA; *Anxa5intron4up:* 5′-CCTGTACTCTATCACTATCACTGACTGTTAATC) and the mutant allele (*Anxa5Ex3dw:* 5′-CGAGAGGCACTGTGACTGACTTCCCTGGAT; *LacZ2up:* 5′-GCCAGTTTGAGGGGACGACGACAG) of the *Anxa5* locus or the wild-type (*Anxa6Intron3dw:* 5′-CACTGTCCTTTGAGCCATCTGCGTCTG; *Anxa6Intron4up:* 5′-GTTGTTGGTGCCCTAGCTGGAAAAAGTCAT) and the mutant allele (*Anxa6Intron3dw:* 5′-CACTGTCCTTTGAGCCATCTGCGTCTG; *Neo2:* 5′-CATCGCCTTCTATCGCCTTCTTGACG) of the *Anxa6* locus. PCR reactions were performed as described previously.[15]

Immunoblotting

Growth plates from femora and tibiae of 13-day-old mice were isolated and homogenized on ice in RIPA lysis buffer, as described previously.[15] After centrifugation at 16,100 × *g* for 30 minutes at 4°C, the supernatant was collected, and the protein concentration was determined by Bradford's protein assay.[17] Equal amounts of protein were separated by SDS-PAGE and transferred onto a nitrocellulose membrane (Whatman, Schleicher & Schuell). Immunostaining was performed with primary rabbit polyclonal antibodies detecting AnxA2 (1:2000; gift of Stephen Moss, London), AnxA5 (1 μg/mL; Hyphen BioMed), AnxA6 (2 μg/mL, Santa Cruz Biotechnology), and a monoclonal mouse antibody detecting actin (0.5 μg/mL; Chemicon). These antibodies were detected subsequently by species-specific secondary antibodies labeled with horseradish peroxidase (DAKO) and were visualized by chemoluminescence using standard procedures.

Whole-mount histologic stainings of newborn mice

Dissection of newborn skeletons and detection of cartilaginous and bony elements by alcian blue and alizarin red S staining were performed as described previuosly.[18]

Histology and immunohistochemistry

Hindlimbs from newborns and femora from 13- and 28-day-old male mice were isolated by dissection and fixed overnight in 4% paraformaldehyde at 4°C. The femora were decalcified in 0.5 M EDTA for 3 weeks at 4°C. All tissues were embedded in paraffin according to standard procedures.[19] Microtome sections (5 μm) of tissues were cut and used for histologic and immunohistochemical analysis. Briefly, for morphologic assessment, sections were stained for mineral deposits (von Kossa, brown or alizarin red S, red), proteoglycans (safranin O, orange/red, or alcian blue, blue), nuclei (hematoxylin, blue/black), and cytoplasm (fast green, blue/green or eosin, red), as described previously.[20] For immunohistochemical analysis, the following antibodies were used: a monoclonal mouse antibody directed against collagen II (10 μg/mL, IgG1 isotype; Calbiochem) and its IgG1 isotype control (Zymed), an affinity-purified rabbit antibody against the NC4 domain of mouse collagen IX (1:2000)[21] and an affinity-purified nonspecific rabbit antibody (1:2000), a rabbit polyclonal antibody against bovine COMP (1:1000)[22] and a rabbit preimmune serum for control (1:1000), an undiluted supernatant of the mouse monoclonal hybridoma clone X53 identifying human collagen X,[23] and an undiluted nonspecific hybridoma supernatant. Corresponding goat-antimouse or goat-antirabbit secondary antibodies coupled to Alexa Fluor 546 or Alexa Fluor 488 (2 μg/mL; Invitrogen/Molecular Probes) were applied. Brightfield as well as fluorescence images were taken (Nikon Eclipse TE2000-U Microscope) and analyzed using the NIS-Elements software (Nikon).

Ultrastructural analysis

Femora of 13-day-old mice were fixed in 2.5% glutaraldehyde in 0.1 M phosphate buffer (pH 7.4) for 24 hours at 4°C, postfixed in 1% buffered osmium tetroxide, and processed for embedding in

epoxy resin (Fluka/BioChemika). Ultrathin sections were analyzed by transmission electron microscopy (LEO 906E, Oberkochen; Germany).

Peripheral quantitative computed tomography (pQCT)

The XCT Research M scanner with software 5.50 (Stratec Medizintechnik, Germany) was used to analyze trabecular and cortical bone, as described previuosly.[20] In brief, right or left femora were scanned at the distal metaphysis (at 15%, 17.5%, and 20% of total bone length measured from the distal joint line) and at the midshaft (at 50% of total bone length). The pixel size was 70×70 μm, with a slice thickness of 500 μm. Parameters derived at the metaphysis (mean of the three slices) included trabecular cross-sectional area (Tb.CSA, mm^2), trabecular bone mineral content (Tb.BMC, mg), and trabecular bone mineral density (Tb.BMD, mg/cm^3). The cortical cross-sectional area (Ct.CSA, mm^2), cortical bone mineral content (Ct.BMC, mg), cortical bone mineral density (Ct.BMD, mg/cm^3), cortical thickness (mm), and the periosteal (mm) and endosteal (mm) circumference of the midshaft were determined. A nonparametric Kruskal-Wallis test was performed to identify differences between genotypes of the same age and gender (SPSS, $p < .05$). Data are presented as mean, and the standard deviation is indicated.

RNA isolation and amplification

Total RNA of the prehypertrophic and hypertrophic zone from cartilage of 13-day-old mouse femora was isolated as described.[24] Briefly, femora were embedded in Tissue-Tek (Sakura Fine Technical), and sections (5 μm) were prepared using a cryostat (Leica CM1850), dehydrated in a series of graded alcohols, and air dried. Prehypertrophic and hypertrophic zones were dissected using an ophthalmic scalpel immobilized on an inverted microscope (Leica DM IL). The RNA of the microdissected samples was extracted using the RNAeasy Micro kit (Qiagen), and the integrity of the RNAs was assessed by capillary electrophoresis (Bioanalyzer, Agilent) according to the specifications of the manufacturer. RNA samples with an RNA integrity number (RIN) value above 8 were considered nondegraded. Samples were amplified (Ambion) in two rounds of linear amplification, as described previously.[25] Amplified RNA samples were fluorescently labeled with either Cy3 or Cy5 fluorophores (Amersham) and used for microarray analysis or for reverse transcription to cDNA using the Superscript III First Strand Synthesis kit (Invitrogen) for downstream qPCR analysis.

Microarray analysis

44K whole genome arrays (Agilent) were hybridized according to the instructions of the manufacturer and subsequently analyzed using an Axon 4000B scanner and the GenePix Pro 4.1 software (Axon Instruments). The primary data then were normalized using the LimmaGUI software package (http://bioinf.wehi.edu.au/limma/), and genes were ranked according to their differential expression and their B-statistic values (Bayes approach). The Gene Ontology Project classification system (www.pantherdb.org) and the available literature were used to classify the proteins according to their function.

Quantitative PCR (qPCR)

Gene-specific primers and prevalidated probes of the universal probe library (Roche) were applied for the genes *Anxa1* to *Anxa7* as well as *Mapk7*. qPCRs were performed using the Platinum qPCR SuperMix-UDG kit (Invitrogen). Reactions were downscaled to 25 μL, and the qPCR was conducted on DNA engine Opticon 2 system (Biorad) as follows: 50°C for a 2-minute hold, 95°C for a 2-minute hold, and 50 cycles of 95°C for 15 seconds and 60°C for 30 seconds. For each primer-probe pair, the efficiency was determined, and the relative fold change was analyzed using the delta-delta CT method.[26,27] *Mapk7,* a gene that is not differentially expressed within the distinct maturation zones of the growth plate, was used for normalization.[24]

Results

AnxA5 and AnxA6 are absent in Anxa5$^{-/-}$Anxa6$^{-/-}$ mice

Anxa5$^{-/-}$*Anxa6*$^{-/-}$ mice were generated by breeding single-gene-deficient *Anxa5*$^{-/-}$[15] and *Anxa6*$^{-/-}$[13] mice on C57BL/6x129SvJ genetic background. A typical analysis of the genotype by PCR analysis is shown for wild type, heterozygous, and double-deficient mice (Fig. 1*A*). The ablation of both annexins was confirmed by immunoblot analysis of growth plate tissue extracts from 13-day-old mice (see Fig. 1*B, arrowheads*). *Anxa2,* which is known to be expressed in growth plate cartilage,[28,29] was detected in similar amounts in wild-type and mutant mice. *Anxa5*$^{-/-}$*Anxa6*$^{-/-}$ mice were viable, and they displayed no

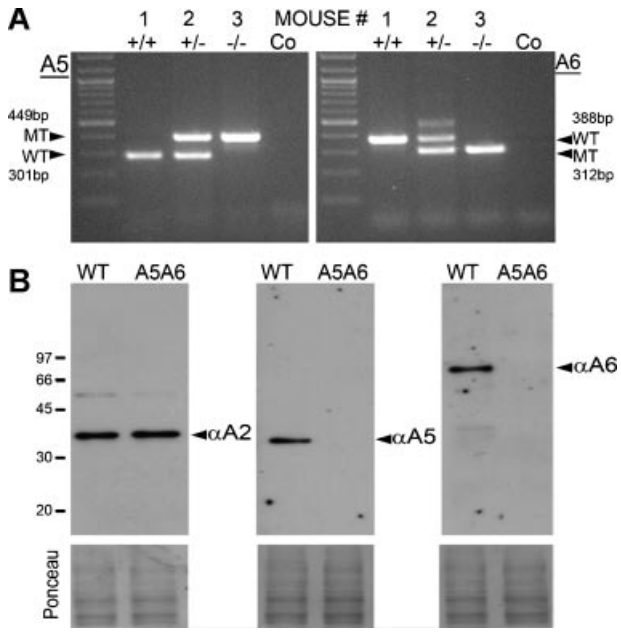

Fig. 1. Annexins A5 and A6 are absent in *Anxa5*$^{-/-}$*Anxa6*$^{-/-}$ mice. (*A*) Genotyping of mutated alleles for *Anxa5* (*left*) and *Anxa6* (*right panel*) by PCR. The corresponding PCR products for wild-type (+/+, WT), heterozygous (+/–), or homozygous mutants ($^{-/-}$, MT) are shown for mice 1 to 3, as indicated. The negative controls (Co) contain no genomic DNA. The size of the resulting PCR fragments is indicated. (*B*) Growth plate extracts of 13-day-old wild-type (WT) and *Anxa5*$^{-/-}$*Anxa6*$^{-/-}$ mutants (A5A6) were tested for the presence of annexin A2 (38.7 kDa), A5 (35.8 kDa), and A6 (75.9 kDa) by immunoblotting. Arrowheads highlight the corresponding protein bands. Ponceau S staining was used as loading control.

obvious phenotypic abnormalities. They also were fertile, because they could be intercrossed to produce normal litter sizes and vital offspring. Intercrosses of *Anxa5*$^{-/-}$*Anxa6*$^{-/-}$ mutant mice showed a normal Mendelian inheritance pattern in 287 live offspring, with the expected ratios of *Anxa5*$^{-/-}$*Anxa6*$^{+/+}$ (26%), *Anxa5*$^{-/-}$*Anxa6*$^{+/-}$ (45%), and *Anxa5*$^{-/-}$*Anxa6*$^{-/-}$ (29%) littermates.

The skeletons of Anxa5$^{-/-}$Anxa6$^{-/-}$ newborn mice develop normally

The development of the skeletal system in newborns was assessed by standard histologic staining techniques to evaluate any alteration in the arrangement, expansion, or mineralization of skeletal elements. Alizarin red S/alcian blue staining of newborns ($n = 4$ per genotype) indicated that the distribution and assembly of the bony (red) and cartilaginous (blue) structures in double-deficient mice (Fig. 2*B*) was indistinguishable from wild type (see Fig. 2*A*). Moreover, length measurements of the bony alizarin red S–positive regions of forelimbs (see Fig. 2*C*) and hindlimbs (see Fig. 2*D*) revealed no significant differences in length compared with wild type. The histomorphology of growth plate cartilage was further analyzed by von Kossa staining to detect mineral deposits and safranin O staining to identify proteoglycans of the cartilaginous tissues of the femur and tibia, respectively. In-plane matched sections did not reveal any significant differences between mutant and wild-type mice in the expansion or morphology of the calcifying hypertrophic zone in overviews (see Fig. 2*E, F, black lines*), as well as at higher magnification (see Fig. 2*G, H, black lines*). Von Kossa staining of mineralized structures (brown stain) confirmed normal mineral deposition in the trabecular structures of mutant mice, and the proteoglycan (orange stain) distribution in *Anxa5*$^{-/-}$*Anxa6*$^{-/-}$ newborns resembled the wild-type situation (see Fig. 2*E–H*).

The growth plate cartilage of juvenile mutant mice displays no alterations in morphology and collagen distribution

The influence of *Anxa5*$^{-/-}$*Anxa6*$^{-/-}$ deficiency on the maturing growth plate was analyzed in 13-day-old mice. In-plane matched sections ($n = 5$) were stained by hematoxylin and eosin, as well as alcian blue, and assessed by microscopical analysis (Fig. 3*A–D*). No differences in the organization of chondrocytes or in the thickness of the growth plate between wild-type (see Fig. 3*A*), single *Anxa5*$^{-/-}$ or *Anxa6*$^{-/-}$ (see Fig. 3*B, C*), or *Anxa5*$^{-/-}$*Anxa6*$^{-/-}$ mice (see Fig. 3*D*) were detectable. Furthermore, deposition of the main interaction partners of both annexins, collagen II and collagen X, was studied in detail by immunofluorescence analysis of the femoral growth plate ($n = 5$ per genotype). Distribution of collagen II (see Fig. 3*E–H, green*) in single-deficient *Anxa5*$^{-/-}$ or *Anxa6*$^{-/-}$ (see Fig. 3*F, G*), as well as in *Anxa5*$^{-/-}$*Anxa6*$^{-/-}$ mice (see Fig. 3*H*), resembled the wild-type situation (see Fig. 3*E*). The protein mostly was restricted to the extracellular matrix of the cartilage (see Fig. 3*E, arrowheads*), and within the growth plate, collagen II staining decreased toward the prehypertrophic and hypertrophic zones. Collagen X protein deposition in the growth plate was indistinguishable between wild-type and mutant mice (see Fig. 3*I–L, red*) and was concentrated mainly in the intercolumnar space of the hypertrophic zone (see Fig. 3*I, arrowheads*).[4] Quantification of the collagen X immunofluorescence-positive area from in-plane matched sections of the right femur of five individual mice per genotype revealed no differences in the distribution (area) of the collagen X protein between 13-day-old wild-type (173.8 ± 7 $\mu m^2 \times 10^3$), single-gene-deficient (*A5*$^{-/-}$ 171 ± 17 $\mu m^2 \times 10^3$, *A6*$^{-/-}$ 175 ± 10 $\mu m^2 \times 10^3$), and *Anxa5*$^{-/-}$*Anxa6*$^{-/-}$ mice (174 ± 7 $\mu m^2 \times 10^3$). The distribution of characteristic proteins associated with collagen fibrils such as collagen IX (see Fig. 3*M, N*) and COMP (see Fig. 3*O, P*) was not altered in mutant mice, and they were found to be localized throughout the growth plate and in the non–growth plate cartilage.[20] Immunostainings with corresponding control antibodies were performed on lateral and medial sections of wild-type femora and confirmed the specificity of all antibodies used in these experiments (Fig. 4).

Organization of the growth plate and mineralization of the skeleton of adult mice is not affected by deficiency of annexins A5 and A6

The morphology of the femoral growth plate was assessed in 1-month-old wild-type and mutant mice using standard histologic staining procedures. In-plane matched sections of males ($n = 3$) were stained by hematoxylin and eosin and alcian blue (Fig. 5*A*) to evaluate the growth plate organization. No significant differences in the thickness of the growth plate, the arrangement of the chondrocytes, and the expansion of the proliferative, prehypertrophic, or hypertrophic zone between wild-type and *Anxa5*$^{-/-}$*Anxa6*$^{-/-}$ mice were found. Femora of 1- and 3-month-old wild-type, *Anxa5*$^{-/-}$, *Anxa6*$^{-/-}$, and *Anxa5*$^{-/-}$*Anxa6*$^{-/-}$ mice also were analyzed by peripheral quantitative computed tomography (pQCT) to determine the degree of biomineralization.[20] The distal metaphysis of each femur ($n = 5$ to 9 per group) was scanned (see Fig. 5*B*) to evaluate the trabecular cross-sectional area (Tb.CSA, *top panel*) as well as the bone mineral content (Tb.BMC, *central panel*) and density (Tb.BMD, *bottom panel*). All parameters were unaffected in 1-month-old mice irrespective of their gender and genotype. This was confirmed by statistical analysis using a nonparametric Kruskal-Wallis test ($p < .05$) showing that for none of the analyzed parameters was a significant difference detected between wild-type and mutant mice. In 3-month-old males ($n = 5$ to 9), the variability of the measured values for trabecular cross-sectional area, bone mineral content, and density increased between individual mice, but between the cohort of distinct genotypes, no significant ($p < .05$) differences were observed. To assess the cortical thickness, the periosteal circumference and endosteal circumference of the femora of the midshaft region were scanned, but the results did not reveal any differences between wild-type, *Anxa5*$^{-/-}$, *Anxa6*$^{-/-}$, and *Anxa5*$^{-/-}$*Anxa6*$^{-/-}$ mice (not shown). Hence total mineralization and structure of the femur were not affected in *Anxa5*$^{-/-}$*Anxa6*$^{-/-}$ mice.

Matrix vesicles are distributed normally in the growth plate of Anxa5$^{-/-}$Anxa6$^{-/-}$ mice

During bone mineralization, calcifying matrix vesicles are essential to initiate the calcification process in hypertrophic

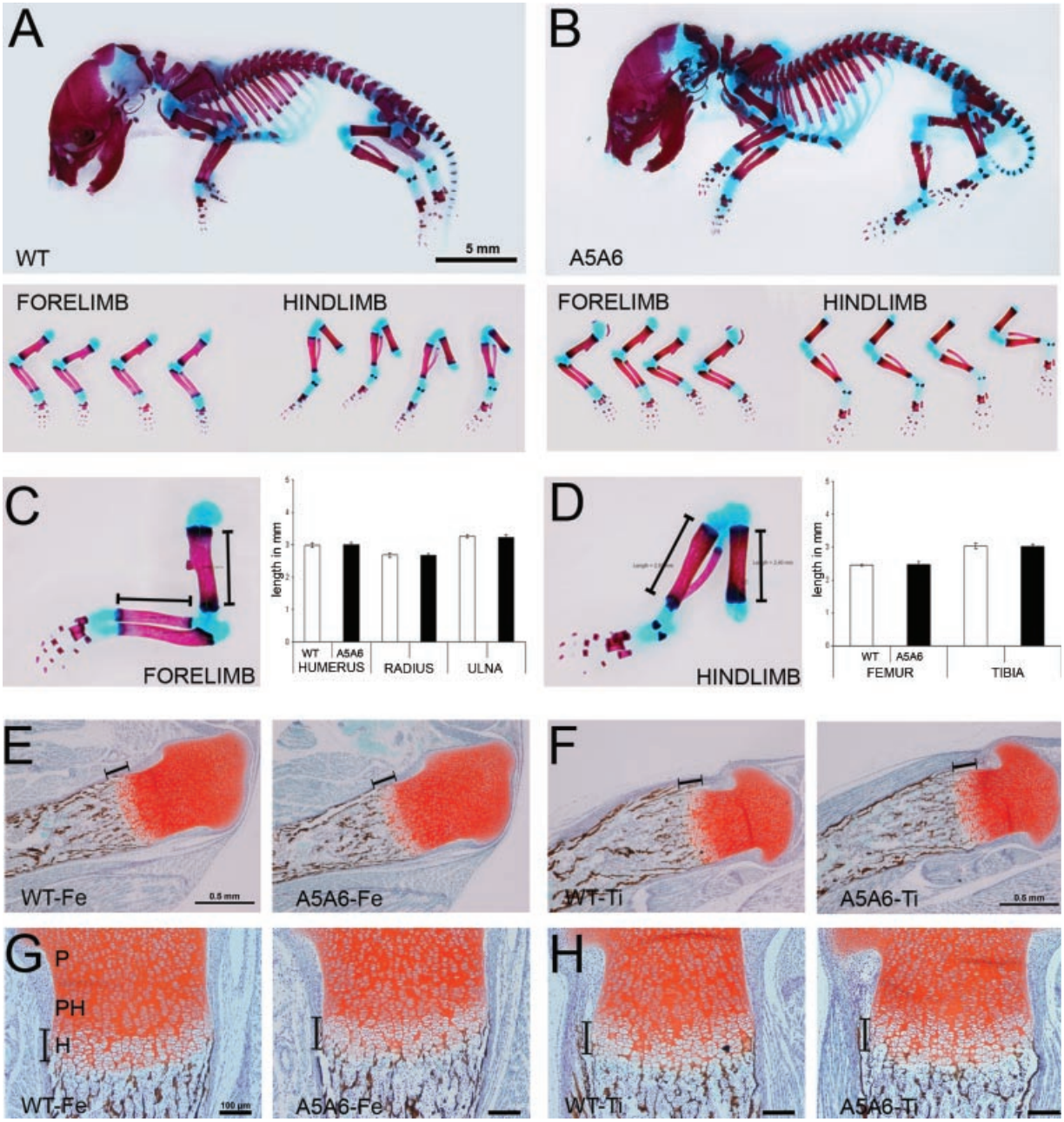

Fig. 2. Cartilaginous and bony elements are distributed normally in wild-type (WT) and *Anxa5*$^{-/-}$*Anxa6*$^{-/-}$ mice (A5A6). (*A, B*) Whole-mount alizarin red S/alcian blue staining of wild-type (*A*) and *Anxa5*$^{-/-}$*Anxa6*$^{-/-}$ (*B*) mice highlights cartilaginous (blue) and bony (red) structures within the skeleton. The individual forelimbs and hindlimbs of four newborn mice per genotype are shown. (*C, D*) The length of the bony elements (i.e., humerus, radius, ulna, femur, and tibia) was measured for each individual extremity (*lines*). The data for wild-type and *Anxa5*$^{-/-}$*Anxa6*$^{-/-}$ mice are presented next to the corresponding limbs within the graphs and show no significant length differences between the genotypes. (*E–H*) In-plane matched sections of femur (Fe) and tibia (Ti) from newborn mice were stained in parallel for mineral deposits (von Kossa, brown), proteoglycans (safranin O, orange/red), nuclei (hematoxylin, blue/black), and cytoplasm (fast green, blue/green). The calcifying hypertrophic zone is marked in each section (*E–H, black line*), and the proliferative (P), prehypertrophic (PH), and hypertrophic (H) zones are indicated (*G*). Bars: 5 mm (*A, B*), 0.5 mm (*E, F*), 100 μm (*G, H*).

growth plate cartilage.[2] In order to define any alteration of matrix vesicle distribution in mutant mice, ultrathin sections of growth plates from 13-day-old mice were analyzed by transmission electron microscopy (Fig. 6). Matrix vesicles were absent in the proliferative zone of wild-type, single-deficient (not shown), and *Anxa5*$^{-/-}$*Anxa6*$^{-/-}$ mice ($n = 4$). No obvious changes in cell morphology or territorial matrix were observed (see Fig. 6*A, D*). In the hypertrophic zone of wild-type or *Anxa5*$^{-/-}$*Anxa6*$^{-/-}$ mice, chondrocytes display a normal morphology, and the mineralization of the interterritorial matrix commences in the expected longitudinal septa between the columns of the cells (see Fig. 6*B, E, arrowheads*), although individual variations in the assembly of the calcifying areas of wild-type as well as *Anxa5*$^{-/-}$*Anxa6*$^{-/-}$ mice were detected. At higher magnification of the calcifying areas (enlargement of the framed regions in Fig. 6*B, E*) in wild-type mice, the needle-like expansion of the

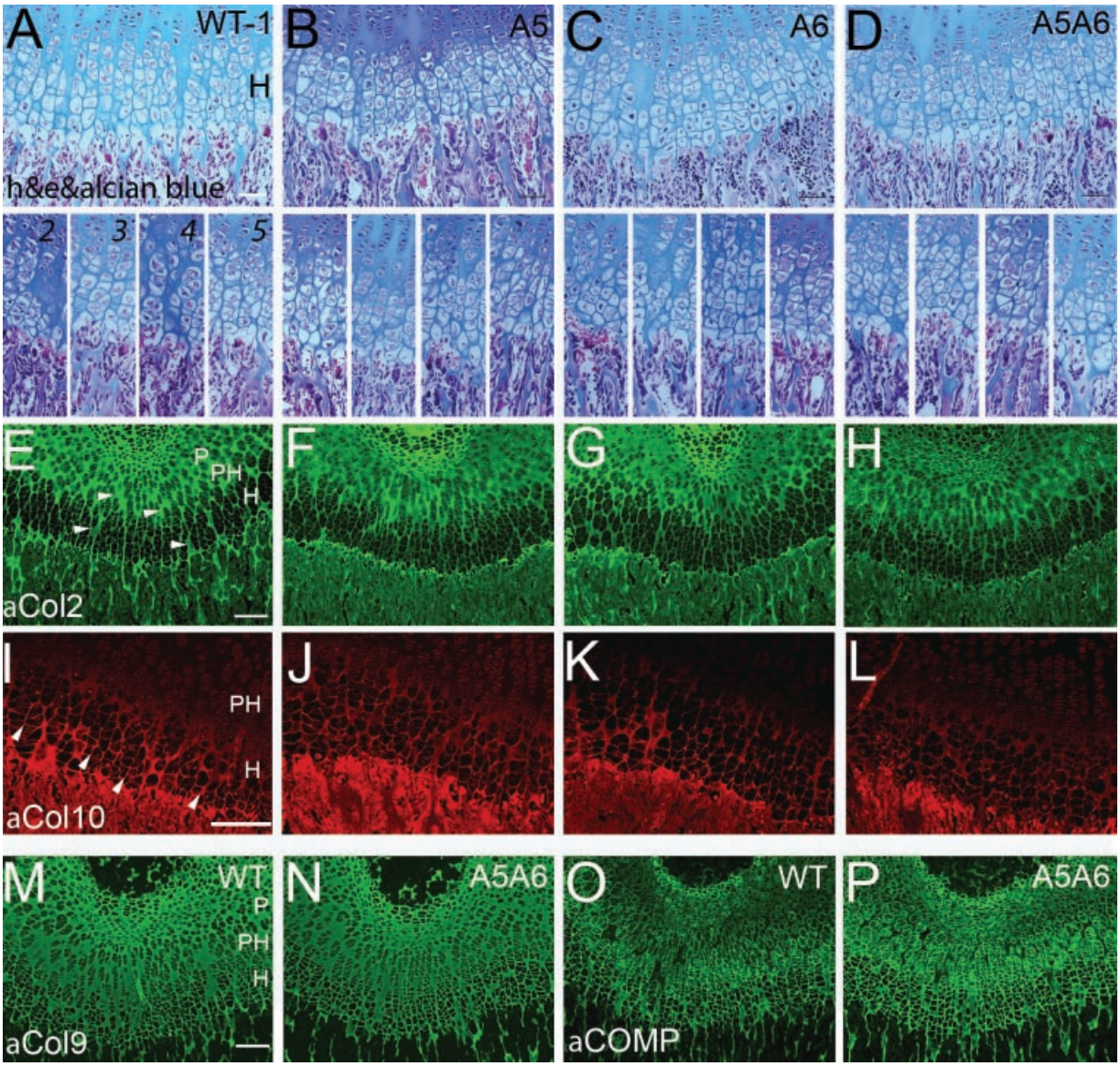

Fig. 3. Overall morphology and collagen distribution are not affected in *Anxa5*$^{-/-}$*Anxa6*$^{-/-}$ growth plates on day 13. (*A–D*) Histology of in-plane matched sections from five femora (1 to 5) of wild-type (*A*), *Anxa5*$^{-/-}$ (*B*), *Anxa6*$^{-/-}$ (*C*), and *Anxa5*$^{-/-}$*Anxa6*$^{-/-}$ (*D*) male mice was assessed using hematoxylin (nuclei, purple), alcian blue (proteoglycans, blue), and eosin (cytoplasm, red) staining. (*E–H, green*) Collagen II protein was detected by immunostaining (aCol2) in paraffin sections from growth plate cartilage of wild-type and mutant mice. Arrowheads point to the extracellular localization of collagen II (*E*). (*I–L, red*) Collagen X protein was localized in the hypertrophic zone of the growth plate from wild-type as well as mutant mice by immunodetection (aCol10), and arrowheads depict the intercolumnar deposition of collagen X in the hypertrophic zone (*I*). Similarly, collagen IX (*M, N*) and COMP (*O, P*) distribution was analyzed by immunostaining of wild-type and *Anxa5*$^{-/-}$*Anxa6*$^{-/-}$ mice. The locations of the proliferative (P), prehypertrophic (PH), and hypertrophic zones (*H*) are highlighted, and the corresponding antibody controls are shown in Fig. 4. Bars: 100 μm.

growing black crystals (see Fig. 6*C*) originating from matrix vesicles is clearly seen. Similar structures are formed in single-deficient (not shown) and *Anxa5*$^{-/-}$*Anxa6*$^{-/-}$ mice (see Fig. 6*F*), indicating that matrix vesicle–mediated biomineralization is initiated properly in *Anxa5*$^{-/-}$*Anxa6*$^{-/-}$ mice.

The remaining annexins are not differentially regulated in Anxa5$^{-/-}$Anxa6$^{-/-}$ mice

These data suggest that annexin A5/A6 double deficiency does not impair skeletal development in mice, although both annexins are expressed in growth plate cartilage. Other genes may compensate for the deficiency of both annexins, and to identify such genes, we analyzed the transcriptome (see Fig. 7*A*) of *Anxa5*$^{-/-}$*Anxa6*$^{-/-}$ mice compared with wild-type mice. The prehypertrophic zone of two wild-type and two mutant mice (see Fig. 7*B*) were microdissected from serial cryosections of the femoral growth plate of 13-day-old male mice. Within these prehypertrophic chondrocytes, the essential cellular programs for initiating biomineralization become activated. The quality of the isolated total RNA from wild-type and *Anxa5*$^{-/-}$*Anxa6*$^{-/-}$ mice was confirmed by microcapillary gel electrophoresis (see Fig. 7*C*), and only high-quality RNA samples were amplified in two rounds of linear RNA amplification.[25] Microarray experi-

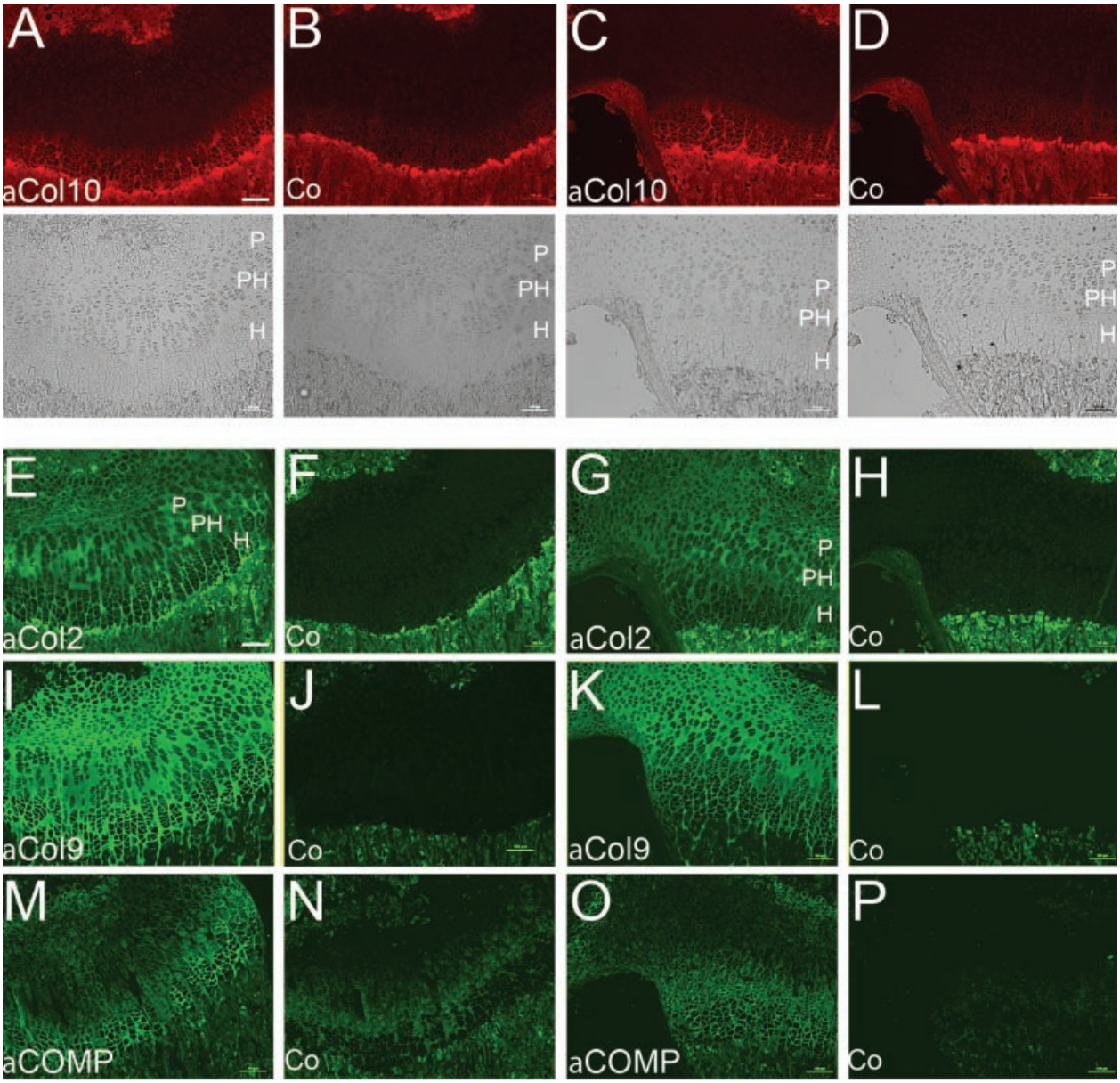

Fig. 4. Assessment of antibody specificity on sections of femoral growth plate cartilage from 13-day-old wild-type mice. Immunostaining of medial (*A, B*) and lateral (*C, D*) sections of the growth plate using the undiluted supernatant of the hybridoma clone X53 (Girkontaite et al., 1996) recognizing collagen X (aCol10) (*A, C*) and the supernatant of a nonspecific hybridoma clone (Co). A diffuse background signal is present in the control staining. The corresponding brightfield images are shown. Collagen II, collagen IX, and COMP were localized by immunodetection in medial (*E, I, M*) and lateral (*G, K, O*) sections. For each antibody, an appropriate primary antibody control was used in similar concentrations, i.e., a nonspecific mouse monoclonal antibody (*F, H,* control), an affinity-purified nonreactive rabbit antibody (*J, L,* control), and a rabbit preimmune serum (*N, P,* control). The locations of the proliferative (P), prehypertrophic (PH), and hypertrophic zones (H) are indicated. Bars: (*A, E*) 100 μm.

ments (Agilent 44K chip) were performed in duplicate for two independent RNA isolations, each derived from an individual wild-type and *Anxa5*$^{-/-}$*Anxa6*$^{-/-}$ mouse. In the overall summary of the experiment, the mean signal intensity (logarithmic scale) for each of the 44,000 probes was plotted against its relative expression levels (see Fig. 7*D*). Genes that were more highly expressed in *Anxa5*$^{-/-}$*Anxa6*$^{-/-}$ mice were found on the positive scale, whereas genes that were more highly expressed in wild-type mice were located on the negative scale of the fold change.

Initially, we focused on the analysis of the 10 members of the annexin family remaining in mutant mice (see Fig. 7*E*). Owing to the highly conserved structures of the annexins, the individual members may fulfill redundant functions that potentially could be indicated by a differential expression of individual annexins. As expected, mRNA levels of *Anxa5* and *Anxa6* were decreased in the *Anxa5*$^{-/-}$*Anxa6*$^{-/-}$ mice, but surprisingly, none of the other annexins were differentially expressed in mutant mice. This was further confirmed by quantitative RT-PCR analysis for the genes *Anxa1* to *Anxa7* using cDNAs generated from amplified prehypertrophic RNA samples of wild-type and *Anxa5*$^{-/-}$*Anxa6*$^{-/-}$ mice (see Fig. 7*E*). No signal was detectable for AnxA9 or AnxA13, and no suitable quantitative RT-PCR assays were available for AnxA8, AnxA10, or AnxA11. Hence, at the mRNA level, no compensation based on differential expression

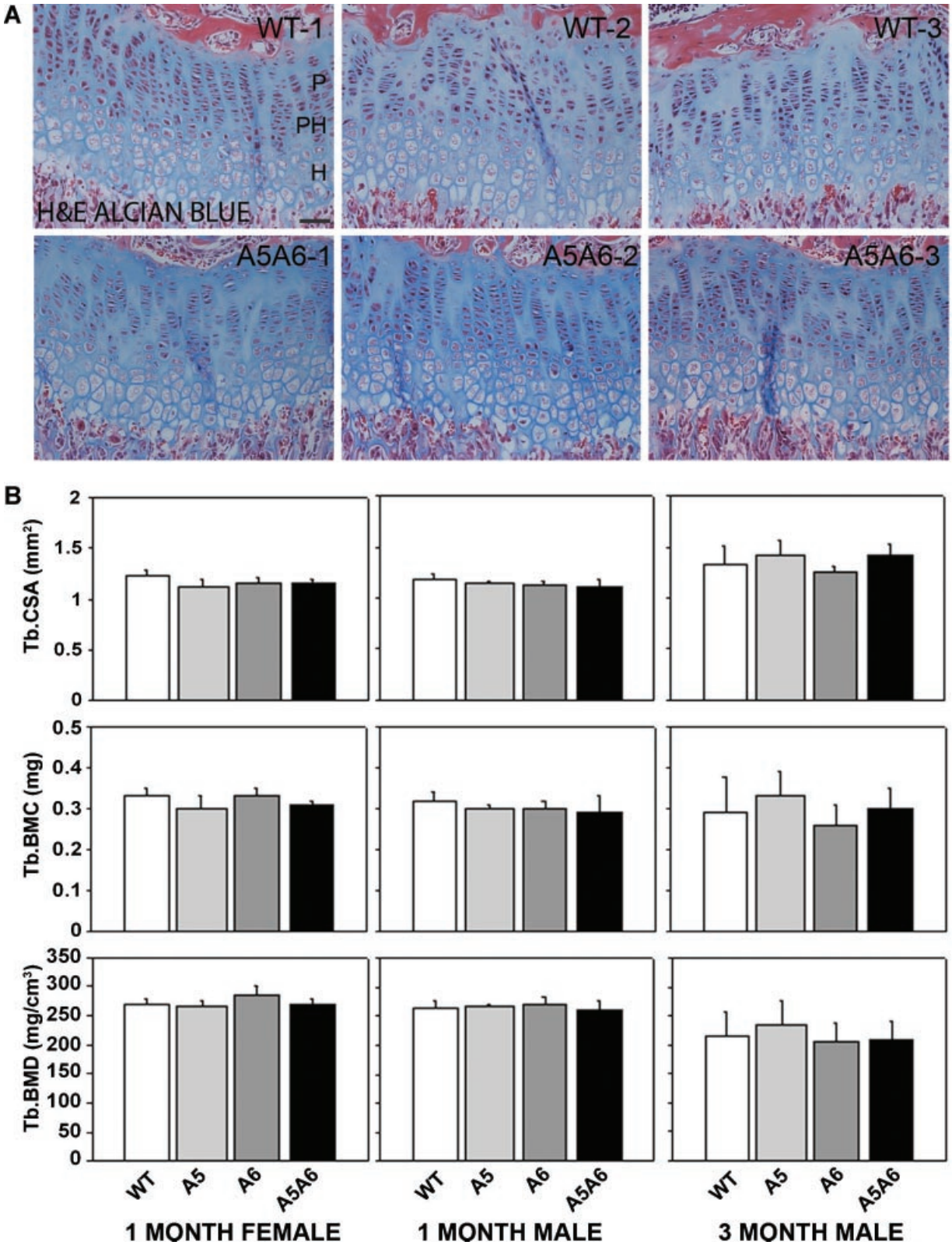

Fig. 5. Growth plate organization and mineral bone content of *Anxa5*$^{-/-}$*Anxa6*$^{-/-}$ mice are not altered in mutant mice. (*A*) Histology of in-plane matched sections from three femora of wild-type (*upper row*) and *Anxa5*$^{-/-}$*Anxa6*$^{-/-}$ (*lower row*) male mice at day 28 were analyzed using hematoxylin (nuclei, purple), eosin (cytoplasm, red), and alcian blue (proteoglycans, blue) stains. (*B*) Peripheral quantitative computed tomography (pQCT) was applied to analyze femoral development in wild-type and mutant mice. Trabecular cross-sectional area (Tb.CSA, *top row*), trabecular bone mineral content (Tb.BMC, *central row*), and trabecular bone mineral density (Tb.BMD, *bottom row*) were determined by pQCT for wild-type (WT), *Anxa5*$^{-/-}$ (A5), *Anxa6*$^{-/-}$ (A6), and *Anxa5*$^{-/-}$*Anxa6*$^{-/-}$ mice (A5A6). No statistical differences ($p < .05$, Kruskal-Wallis test) were detected between groups in female (1-month-old) and male (1- and 3-month-old) mice ($n = 5$ to 9 animals for each genotype).

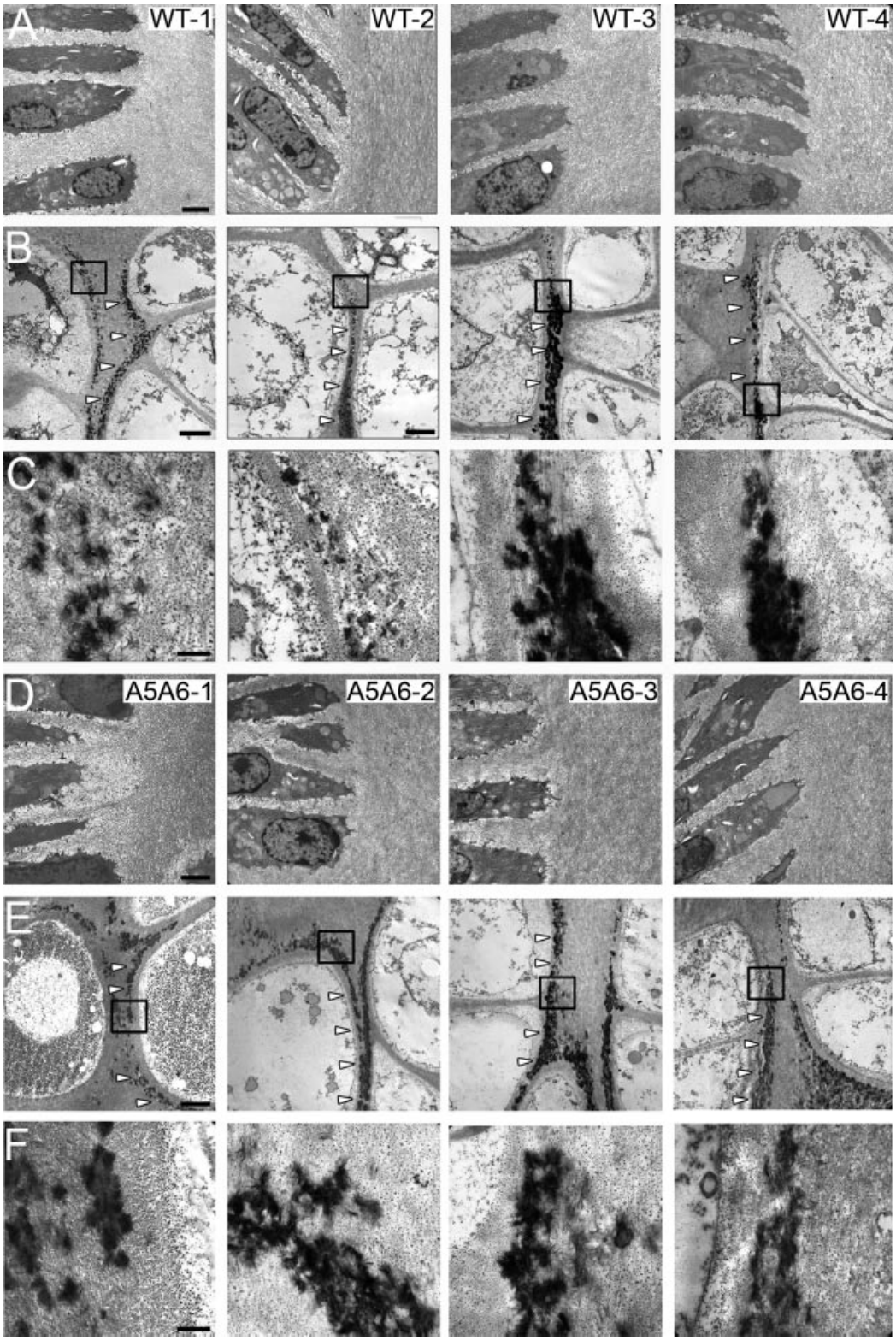

Fig. 6. Distribution of matrix vesicles in the intercellular space of the hypertrophic zone of growth plate cartilage is not altered in 13-day-old wild-type and mutant mice. (*A–F*) Growth plate morphology from four individual wild-type (WT, *A–C*) and *Anxa5*$^{-/-}$*Anxa6*$^{-/-}$ mice (A5A6, *D–F*) were analyzed by electron microscopy. Cells from the proliferative (*A, D*) and hypertrophic (*B, E*) zones are shown, and the calcifying areas of the interterritorial matrix are marked by arrowheads. Squares within the images of the hypertrophic zone indicate the magnified regions of interest, which are shown in *C* and *F*. Accumulations of electron-dense black material in the intercellular region of hypertrophic cells (*C, F*) correspond to hydroxyapatite crystals that originate from a matrix vesicle. Bars: 2 μm (*A, D*), 3.5 μm (*B, E*), 500 nm (*C, F*).

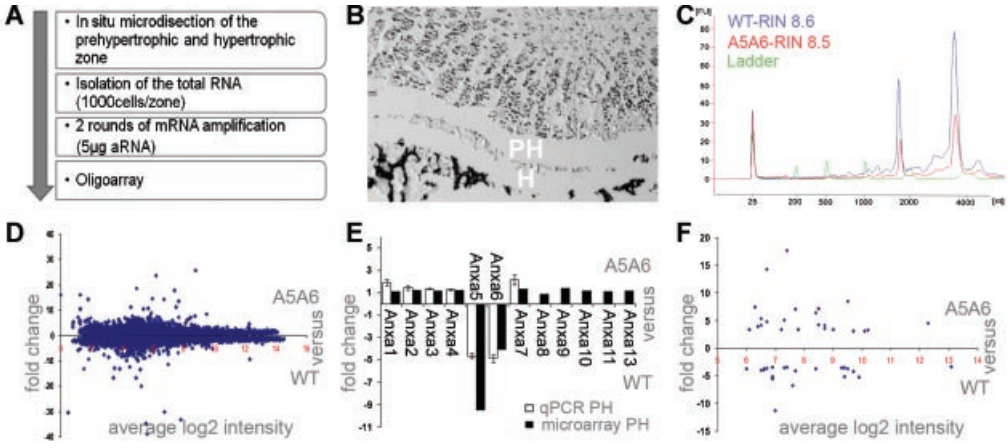

G

upregulated genes	fold change *(≥ 3)*	mean intensity *(≥ 6)*	B *(≥ 1)*	function
Depdc6	25,8	8,8	3,2	?
Ptdsr	17,7	7,4	2,7	1, 3, 11
Pold3	14,3	6,7	4,6	1
8430408G22Rik	8,5	9,5	3,6	?
Metapl1	7,5	6,3	3,7	1, 2
1110007A13Rik	7,2	8,5	2,9	?
Mod1	7,1	7,7	2,7	6, 10
Rpgrip1	6,5	8,4	3,4	1, 2, 12
Cdkn3	5,4	6,5	2,3	2
Cbr1	5,1	7,3	2,9	10
Napa	4,8	6,7	3,1	16
Slc1a5	4,6	12,3	2,6	3, 4, 9
Ttc3	4,3	8,5	1,7	1, 12
AK034071	4,2	6,5	1,7	?
Mrps12	4,2	8,7	1,4	1
Tanc1	4	6,4	2,6	?
Npr3	3,6	8,7	1,3	1, 12
Pttg1	3,4	9,0	1,6	1, 3
Rnf41	3,4	6,1	1,8	1, 5
Pop1	3,4	7,8	1,5	14
Ppp1r14a	3,4	7,2	1,6	1
Vegfa	3,3	10,2	1,2	1, 13
Trib3	3,1	10,1	1,6	1, 3
TC1537584	3,1	9,7	1,3	?

downregulated genes	fold change *(≤ -3)*	mean intensity *(≥ 6)*	B *(≥ 1)*	function
BC045135	-33,1	7,8	2,1	?
NAP115274-1	-30,1	6,8	3,1	?
Unc13a	-11,3	7	3,8	1
Eno2	-6,7	7,6	2,8	7
Eraf	-5,5	6,9	3,5	15
Hbb-b1	-5,2	9,9	2,4	16
Epha4	-5,1	6,9	1,8	1
Kras	-5,1	9,4	2,5	1, 4, 12
4933439C20Rik	-4,2	9,7	2,3	10
Acad9	-4,1	7,7	1,9	10
Cox7c	-4	6,5	1,5	9
Tsn	-3,9	6,6	1,5	1
Igf1	-3,7	6	2,5	1, 3, 6, 13
Slc4a1	-3,7	8,4	1,6	16
Rnf111	-3,7	9,5	2,2	1, 10
Arl5c	-3,7	6,6	2,1	?
Slc10a4	-3,6	6,7	1,3	16
E2f2	-3,5	9,4	1,6	2, 4
Gbe1	-3,5	9,3	1,5	8
Vpreb3	-3,5	7,3	1,7	6, 16
AK047664	-3,4	6,9	1,6	?
Tusc3	-3,4	7,4	1,2	4
Acpl2	-3,3	13,1	1	?

function:

cell proliferation (56 %)	intermediate metabolism (19 %)	other biological functions (25 %)
1.cell proliferation and differentiation (18x)	6.glucose homeostasis (2x)	11.lipid and fatty acid binding (1x)
2.cell cycle (4x)	7.glycolysis (1x)	12.G-protein mediated signaling (4x)
3.apoptosis (5x)	8.glycogen metabolism (1x)	13.receptor protein kinase signaling pathway (2x)
4.tumor supressor/survival (4x)	9.Krebs cycle (2x)	14.tRNA metabolism (1x)
5.cell motility (1x)	10.lipid, fatty acid and steroid metabolism (5x)	15.protein folding (2x)
		16.transport (4x)

Fig. 7. Comparison of the transcriptome in the prehypertrophic zone of the growth plate of *Anxa5*$^{-/-}$*Anxa6*$^{-/-}$ and wild-type mice defines complex changes of gene expression. (*A*) The experimental outline of the RNA isolation and amplification protocol for microarray analysis is shown. (*B*) A performed microdissection of the prehypertrophic (PH) and hypertrophic (H) microdomains on a cryosection of the growth plate cartilage from 13-day-old mice is demonstrated. (*C*) Yield, purity, and integrity of the isolated total RNA from wild-type (WT) and *Anxa5*$^{-/-}$*Anxa6*$^{-/-}$ (A5A6) mice were assessed by capillary electrophoresis. (*D*) Expression of mRNA in prehypertrophic zones from growth plates was detected by microarray analysis (Agilent 44K chip), and all genes are plotted as *n*-fold change versus their average expression levels, respectively. (*E*) Microarray data and qPCR analysis (*Anxa1* to *Anxa7*) of annexins are compared and show the high degree of consistency of expression data from both methods. (*F*) Differentially regulated genes are displayed with expression levels above background and significant changes in expression levels (*B* value $\geq$1, average expression $\geq$6, fold change $\geq \pm 3$). (*G*) Individual differentially expressed genes that are either upregulated (*left*) or downregulated (*right*) in mutant mice are listed according to their fold change. For each gene, potential biologic functions according to GO annotation and the literature are indicated by numbers that reflect the biologic process as shown. Differentially expressed genes are classified according to their potential biologic functions (GO annotation and the literature).

was found for any of the tested members of the annexin family in *Anxa5*$^{-/-}$*Anxa6*$^{-/-}$ mice.

Genes involved in cell growth and intermediate metabolism are regulated in mutant mice

In order to identify genes that are potentially influenced by the *Anxa5*$^{-/-}$*Anxa6*$^{-/-}$ deficiency, the data set was selected for genes that are likely to be differentially expressed (*B* value $\geq$1), show a signal intensity above background noise (intensity $\geq$6), and display a more than threefold change in relative expression levels (see Fig. 7*F*). Using these selection criteria, we identified 47 genes that are differentially expressed in *Anxa5*$^{-/-}$*Anxa6*$^{-/-}$ mice compared with wild-type mice. Genes were ranked according to their changes in relative expression levels either to be upregulated (24 genes) or downregulated (23 genes) in *Anxa5*$^{-/-}$*Anxa6*$^{-/-}$ mice (see Fig. 7*G*) and were classified on the basis of their GO annotations (biologic processes), as well as published data. Potentially, other genes that are known to be involved in biomineralization processes could be differentially expressed in mutant mice to compensate for the loss of AnxA5 and AnxA6. However, in the microarray data set, none of these genes, such as matrix Gla protein, ecto-nucleotide pyrophosphatase/phosphodiesterase 1 (*NPPS*) or alkaline phosphatase,[30–32] are regulated. Most regulated genes (56%) are associated with processes relevant to cell growth or differentiation and survival, such as *Ttc3, Pttg1, Ppp1r14a, Trib3, Npr3, Vegfa, Pold3, Kras, Igf1, E2f2,* and *Tusc3*. Nineteen percent of the genes (11 genes) contribute to intermediate metabolism, and one gene, *Ptdsr,* is potentially involved in lipid and fatty acid binding. Some genes coding for proteins participate in G-protein-mediated signaling pathways, and a number of genes are involved in transport processes and contribute to vesicle, protein, or chloride/bicarbonate trafficking. For another 11 differentially expressed genes, a function still has to be described. For validation of the microarray data, the mRNA levels of selected genes such as *Ptdsr,* which is highly differentially expressed (17.7-fold upregulated), and *Vegfa,* which shows only a low differential expression (3.3-fold upregulated), were tested by quantitative RT-PCR. A close correlation was observed to the microarray data, reflected by the significant upregulation for *Ptdsr* (6-fold, not shown) and a less pronounced upregulation of *Vegfa* (3-fold, not shown).

Discussion

Mineralization of growth plate cartilage is mediated by the induction of hydroxyapatite formation in matrix vesicles within the intercolumnar space of hypertrophic chondrocytes in a strictly time- and tissue-specific manner.[2] Mineralization-competent matrix vesicles are crucial to induce biomineralization, and it was postulated that AnxA5 and AnxA6 are key players that promote the calcification of these matrix vesicles.[33]

Previous studies suggested that AnxA5 and AnxA6 act as calcium channels that may induce calcium deposition in matrix vesicles of calcifying tissues on interaction with the extracellular matrix.[6,7,12] These studies mostly relied on biochemical interaction experiments, in vitro mineralization assays, or cell culture studies that cannot be applied directly to the in vivo situation. We therefore generated mice deficient for AnxA5 and AnxA6 and analyzed the mineralization of cartilage by histologic and immunohistochemical methods. None of these methods detected significant changes in the morphology of the growth plate, extracellular matrix protein distribution, or mineral deposition of mutant mice. More important, our ultrastructural analysis demonstrates that growing mineral crystals derived from calcifying matrix vesicles are still formed in the hypertrophic zone of *Anxa5*$^{-/-}$*Anxa6*$^{-/-}$ mice but are absent in the proliferative zone. The number and size of deposited calcifying matrix vesicles vary to a certain degree between individuals of a given genotype (see Fig. 6), but no significant alterations were detected between wild-type or mutant mice. This is in contrast to our expectations because the gene-deficient mouse model of collagen X, the proposed binding partner of annexin A5 and A6, displays major changes in the distribution and organization of growth plate matrix vesicles.[16]

These results show a clear discrepancy between the in vitro findings and the in vivo situation, indicating that AnxA5 and AnxA6 may not be involved in biomineralization processes. Therefore, the in vitro experiments may not be well suited to reflect the in vivo situation or, on the other hand, the mineralization process may represent a stable and robust pathway thatis largely independent of changes in the expression of both genes owing to functional compensation by other proteins involved in biomineralization.

Since annexins exhibit a high degree of structural similarity, which has remained conserved during evolution for more than 1 billion years,[34] it is possible that these proteins may fulfill redundant functions during the biomineralization process. The compensation of the loss of function for AnxA5 and AnxA6 may involve the upregulation of distinct annexins on the mRNA or protein level, but our results did not support this hypothesis. None of the remaining 10 members of the annexin family in *Anxa5*$^{-/-}$*Anxa6*$^{-/-}$ mice were differentially expressed at the mRNA level in transcriptome and quantitative PCR studies of the prehypertrophic growth plate cartilage (see Fig. 7). At the protein level, no altered expression was seen for AnxA2 in immunoblot analysis, whereas for the other members of the annexin family, no suitable antibodies were available to us because several of the tested commercially available antibodies recognize more than one annexin (Brachvogel et al., unpublished results). Therefore, an altered protein expression or intracellular distribution of distinct annexins, e.g., to vesicles, cannot be excluded at this stage of analysis.

Two other annexins, AnxA1 and AnxA8, are expressed as proteins in growth plate cartilage. AnxA1 was identified just recently in calcifying matrix vesicles from femoral chicken embryo using a proteome analysis approach,[28] but its function in growth plate development and homeostasis is largely unknown. AnxA1-deficient mice display no gross differences in the appendicular skeleton. In contrast, a delay in intramembranous ossification of the skull and an incomplete fusion of the sutures was observed in these mice, pointing to a role of AnxA1 in osteoblast differentiation rather than in biomineralization processes during endochondral ossification.[35] AnxA8 was

described previously as being most highly expressed in the hypertrophic zone of the fetal bovine growth plate.[29] The protein is a poorly characterized member of the protein family, and an ion channel function for AnxA8 was postulated mainly based on structure predictions and homology with other annexins.[36,37] Its capacities for binding to extracellular matrix proteins or the potential to form calcium channels still has to be determined. For none of the remaining annexins, an expression within the growth plate or even an influence on skeletal development in vivo could be demonstrated, except for AnxA7. Haploinsufficient *Anxa7*$^{+/-}$ mice exhibit male-specific giantism, indicating that bone growth and biomineralization may depend on AnxA7 expression.[38] However, a detailed analysis of the skeletal phenotype is still pending, and the giantism might be overtly affected by endocrine secretory defects that were identified previously in these mice.[39] Owing to the presence of multiple annexins within the growth plate, the precise function of the individual annexins and their contribution to mineralization processes in the growth plate cannot be defined at this stage. Some members of the annexin family are expressed but not regulated in *Anxa5*$^{-/-}$*Anxa6*$^{-/-}$ mice; they still functionally compensate for the loss of both annexins in these mice. It will be of interest to assess the skeletal phenotype in *Anxa5*$^{-/-}$*Anxa6*$^{-/-}$ mice where other annexins such as AnxA1, AnxA2, AnxA7, AnxA8, or other components of the biomineralization process such as collagen X are additionally deleted.

Alternatively, the discrepancy between in vitro and in vivo data may be explained by the fact that multiple non-annexin-related pathways are involved in the formation of functional bone and that the contributions by annexins A5 and A6 are not essential for endochondral ossification. However, at the level of mRNA expression, we could not identify any genes that were significantly regulated and known to be of relevance for biomineralization, e.g., matrix Gla protein, ectonucleotide pyrophosphatase/phosphodiesterase 1 (NPPS), or alkaline phosphatase.[30–32]

While our data do not support the suggestion that AnxA5 and AnxA6 are crucial regulators for normal bone formation and mineralization in vivo, the in vitro evidence for their potential calcifying activity and their expression at high levels in growth plate cartilage suggest that they are of importance for the formation of a stiff and stable skeletal system. Potentially, *Anxa5*$^{-/-}$*Anxa6*$^{-/-}$ mice may develop a biomineralization-linked phenotype under some challenging conditions that is not apparent under normal conditions. In future studies, loss of estrogen owing to ovariectomy can be used to generate an osteoporosis-like phenotype to simulate postmenopausal bone loss[40] or fractures can be induced to analyze bone-healing processes in these *Anxa5*$^{-/-}$*Anxa6*$^{-/-}$ mice. Both experiments will provide important information about the influence of AnxA5 and AnxA6 on the progression of osteoporosis and bone remodeling processes.

In contrast to members of the annexin family, whole-genome studies indicate that various other genes are affected by the annexin A5/A6 deficiency. This includes genes contributing to cell growth and metabolism as well as to protein synthesis, amino acid transport, and carbohydrate metabolism (see Fig. 7). Hence annexins A5 and A6 potentially may fulfill functions in the growth plate not directly linked to biomineralization, but there are no obvious indications for an underlying regulatory mechanism that causes the differential expression of these genes. It is known that annexins can interact in a calcium-dependent manner with phospholipids to modulate membrane trafficking and thereby link Ca^{2+} signaling to membrane dynamics.[41] In particular, AnxA6 can influence the release of Ca^{2+} from the sarcoplasmatic reticulum,[42] and consequently, the loss of AnxA6 may modulate calcium signaling events within chondrocytes. Otherwise, AnxA5 can raise the intracellular Ca^{2+} levels in osteoblasts in response to mechanical stimuli.[43] The absence of both annexins therefore may interfere with the adequate Ca^{2+} signaling in prehypertrophic chondrocytes and cause the observed complex changes in the expression of multiple transcripts in the mutant growth plate.

In conclusion, we show that the absence of both annexins A5 and A6 does not impair biomineralization of cartilage during enchondral ossification in vivo.

Disclosures

All authors have no conflicts of interest.

Acknowledgments

This project was supported by grants from the Deutsche Forschungsgemeinschaft: BR2304/2-1 and BR2304/4-1. Both Daniele Belluoccio and Ivan Grskovic contributed equally.

References

1. Balcerzak M, Hamade E, Zhang L, et al. The roles of annexins and alkaline phosphatase in mineralization process. Acta Biochim Pol. 2003;50:1019–1038.
2. Anderson HC. Matrix vesicles and calcification. Curr Rheumatol Rep. 2003;5: 222–226.
3. Berendes R, Burger A, Voges D, Demange P, Huber R. Calcium influx through annexin V ion channels into large unilamellar vesicles measured with fura-2. FEBS Lett. 1993;317:131–134.
4. Kirsch T, von der Mark K. Remodelling of collagen types I, II and X and calcification of human fetal cartilage. Bone Miner. 1992;18:107–117.
5. Koopman G, Reutelingsperger CP, Kuijten GA, Keehnen RM, Pals ST, van Oers MH. Annexin V for flow cytometric detection of phosphatidylserine expression on B cells undergoing apoptosis. Blood. 1994;84:1415–1420.
6. Genge BR, Wu LN, Wuthier RE. Kinetic analysis of mineral formation during in vitro modeling of matrix vesicle mineralization: effect of annexin A5, phosphatidylserine, and type II collagen. Anal Biochem. 2007;367:159–166.
7. Genge BR, Wu LN, Wuthier RE. In vitro modeling of matrix vesicle nucleation: synergistic stimulation of mineral formation by annexin A5 and phosphatidylserine. J Biol Chem. 2007;282:26035–26045.
8. Kim HJ, Kirsch T. Collagen/annexin V interactions regulate chondrocyte mineralization. J Biol Chem. 2008;283:10310–10317.
9. Brachvogel B, Pausch F, Farlie P, et al. Isolated *Anxa5*(+)/*Sca-1*(+) perivascular cells from mouse meningeal vasculature retain their perivascular phenotype in vitro and in vivo. Exp Cell Res. 2007;313: 2730–2743.
10. Brachvogel B, Moch H, Pausch F, et al. Perivascular cells expressing annexin A5 define a novel mesenchymal stem cell-like population

with the capacity to differentiate into multiple mesenchymal lineages. Development. 2005;132:2657–2668.

11. Collett GD, Canfield AE. Angiogenesis and pericytes in the initiation of ectopic calcification. Circ Res. 2005;96:930–938.
12. Kirsch T, Harrison G, Golub EE, Nah HD. The roles of annexins and types II and X collagen in matrix vesicle-mediated mineralization of growth plate cartilage. J Biol Chem. 2000;275:35577–35583.
13. Hawkins TE, Roes J, Rees D, Monkhouse J, Moss SE. Immunological development and cardiovascular function are normal in annexin VI null mutant mice. Mol Cell Biol. 1999;19:8028–8032.
14. Ling Q, Jacovina AT, Deora A, et al. Annexin II regulates fibrin homeostasis and neoangiogenesis in vivo. J Clin Invest. 2004;113: 38–48.
15. Brachvogel B, Dikschas J, Moch H, et al. Annexin A5 is not essential for skeletal development. Mol Cell Biol 2003;23:2907–2913.
16. Kwan KM, Pang MK, Zhou S, et al. Abnormal compartmentalization of cartilage matrix components in mice lacking collagen X: implications for function. J Cell Biol. 1997;136:459–471.
17. Bradford MM. A rapid and sensitive method for the quantitation of microgram quantities of protein utilizing the principle of protein-dye binding. Anal Biochem. 1976;72:248–254.
18. Schmitz M, Niehoff A, Miosge N, Smyth N, Paulsson M, Zaucke F. Transgenic mice expressing D469delta mutated cartilage oligomeric matrix protein (COMP) show growth plate abnormalities and sternal malformations. Matrix Biol. 2008;27:67–85.
19. Romeis B, Boeck P. *Mikroskopische Technik*. Berlin, Urban & Schwarzenbeck, 1989.
20. Blumbach K, Niehoff A, Paulsson M, Zaucke F. Ablation of collagen IX and COMP disrupts epiphyseal cartilage architecture. Matrix Biol. 2008;27:306–318.
21. Budde B, Blumbach K, Ylostalo J, et al. Altered integration of matrilin-3 into cartilage extracellular matrix in the absence of collagen IX. Mol Cell Biol. 2005;25:10465–10478.
22. DiCesare P, Hauser N, Lehman D, Pasumarti S, Paulsson M. Cartilage oligomeric matrix protein (COMP) is an abundant component of tendon. FEBS Lett. 1994;354:237–240.
23. Girkontaite I, Frischholz S, Lammi P, et al. Immunolocalization of type X collagen in normal fetal and adult osteoarthritic cartilage with monoclonal antibodies. Matrix Biol. 1996;15:231–238.
24. Belluoccio D, Bernardo BC, Rowley L, Bateman JF. A microarray approach for comparative expression profiling of the discrete maturation zones of mouse growth plate cartilage. Biochim Biophys Acta. 2008;1779:330–340.
25. Van Gelder RN, von Zastrow ME, Yool A, Dement WC, Barchas JD, Eberwine JH. Amplified RNA synthesized from limited quantities of heterogeneous cDNA. Proc Natl Acad Sci USA. 1990;87:1663–1667.
26. Livak KJ, Schmittgen TD. Analysis of relative gene expression data using real-time quantitative PCR and the 2(−δδC(T)) method. Methods. 2001;25:402–408.
27. Pfaffl MW. A new mathematical model for relative quantification in real-time RT-PCR. Nucleic Acids Res. 2001;29:45.
28. Balcerzak M, Malinowska A, Thouverey C, et al. Proteome analysis of matrix vesicles isolated from femurs of chicken embryo. Proteomics. 2008;8:192–205.
29. White AH, Watson RE, Newman B, Freemont AJ, Wallis GA. Annexin VIII is differentially expressed by chondrocytes in the mammalian growth plate during endochondral ossification and in osteoarthritic cartilage. J Bone Miner Res. 2002;17:1851–1858.
30. Karsenty G. The complexities of skeletal biology. Nature. 2003;423: 316–318.
31. Karsenty G. Genetic control of skeletal development. Novartis Found Symp. 2001;232:6–17; discussion 17–22.
32. Murshed M, Schinke T, McKee MD, Karsenty G. Extracellular matrix mineralization is regulated locally: different roles of two gla-containing proteins. J Cell Biol. 2004;165:625–630.
33. Kirsch T. Annexins: their role in cartilage mineralization. Front Biosci. 2005;10:576–581.
34. Morgan RO, Fernandez MP. Molecular phylogeny of annexins and identification of a primitive homologue in *Giardia lamblia*. Mol Biol Evol. 1995;12:967–979.
35. Damazo AS, Moradi-Bidhendi N, Oliani SM, Flower RJ. Role of annexin 1 gene expression in mouse craniofacial bone development. Birth Defects Res A Clin Mol Teratol. 2007;79:524–532.
36. Rety S, Sopkova-de Oliveira Santos J, Dreyfuss L, et al. The crystal structure of annexin A8 is similar to that of annexin A3. J Mol Biol. 2005;345:1131–1139.
37. Hofmann A, Escherich A, Lewit-Bentley A, et al. Interactions of benzodiazepine derivatives with annexins. J Biol Chem. 1998;273: 2885–2894.
38. Srivastava M, Montagna C, Leighton X, et al. Haploinsufficiency of *Anx7* tumor suppressor gene and consequent genomic instability promotes tumorigenesis in the *Anx7(+/–)* mouse. Proc Natl Acad Sci USA. 2003;100:14287–14292.
39. Srivastava M, Atwater I, Glasman M, et al. Defects in inositol 1,4,5-trisphosphate receptor expression, Ca^{2+} signaling, and insulin secretion in the *anx7(+/–)* knockout mouse. Proc Natl Acad Sci USA. 1999;96:13783–13788.
40. Hikiji H, Ishii S, Shindou H, Takato T, Shimizu T. Absence of platelet-activating factor receptor protects mice from osteoporosis following ovariectomy. J Clin Invest. 2004;114:85–93.
41. Gerke V, Creutz CE, Moss SE. Annexins: linking Ca^{2+} signalling to membrane dynamics. Nat Rev Mol Cell Biol. 2005;6:449–461.
42. Hazarika P, Kaetzel MA, Sheldon A, et al. Annexin VI is associated with calcium-sequestering organelles. J Cell Biochem. 1991;46: 78–85.
43. Haut Donahue TL, Genetos DC, Jacobs CR, Donahue HJ, Yellowley CE. Annexin V disruption impairs mechanically induced calcium signaling in osteoblastic cells. Bone. 2004;35:656–663.